

Low SWaP-C Radar for Urban Air Mobility

William A. Lies, Lakshay Narula
Electrical and Computer Engineering
The University of Texas at Austin
Austin, TX, USA
wlies@austin.utexas.edu
lakshay.narula@utexas.edu

Peter A. Iannucci, Todd E. Humphreys
Aerospace Engineering & Engineering Mechanics
The University of Texas at Austin
Austin, TX, USA
peter.iannucci@austin.utexas.edu
todd.humphreys@utexas.edu

Abstract—A method is developed and tested for extending the range of low-cost radar chipsets for use in urban air mobility (UAM) vehicles. The method employs weak-signal correlation techniques and long measurement intervals to achieve a 1 km range. Low-cost radar is an enabling technology for vertical take-off and landing (VTOL) aircraft envisioned for large-scale deployment in urban areas. These aircraft must be autonomously piloted to make them economically feasible, but autonomous systems have yet to match a human pilot’s ability to detect and avoid (DAA) obstacles. Visible light cameras are useful for this application, but cameras alone are insufficient, as they are fundamentally unable to resolve range. Existing commercial radar units would suffice for DAA, but their large size weight, power, and cost (SWaP-C) militates against their application to UAM. The technique detailed in this paper is a fused camera-radar solution that exploits the camera’s excellent angular resolution to guide radar signal processing so that signals arriving from a camera-detected target are combined constructively. Such guided processing significantly extends the range of low SWaP-C radar chipsets, making them useful for DAA. An analysis of the fused technique’s robustness to target velocity uncertainty is presented, along with experimental results indicating that a typically-sized VTOL aircraft would be detectable at a range of 1 km.

I. INTRODUCTION

Urban air mobility (UAM) and urban air logistics (UAL) are the subject of an intense worldwide research and development effort. Existing aerospace companies and start-ups alike are developing small, vertical take-off and landing aircraft (VTOLs) with the goal of offering short-distance air transportation as an alternative to ground transportation for both people (UAM) and products (UAL). These aircraft will eventually be autonomously piloted to reduce cost [1], [2].

Detect and avoid (DAA) is an essential capability for achieving large-scale UAM and UAL [3]. Autonomously-piloted aircraft must be able to reliably see and avoid airborne objects such as conventional aircraft, VTOLs, small delivery drones, and even large birds. This capability is essential when a threatening object is not broadcasting its position (non-cooperative) or during a malfunction of cooperative collision avoidance systems. DAA systems must match or exceed a human pilot’s ability to visually avoid obstacles [4], [5]. Current research is focused on camera-based systems, attractive for their low size, weight, power, and cost (SWaP-C). The fundamental limitation of visual DAA systems is their inability to accurately resolve range. Thus, cameras alone are not sufficient for reliable DAA. A capable radar system with low SWaP-C would provide a

fundamental complement to visual sensing for autonomous DAA, since radar has excellent range discrimination. This work explores signal processing techniques for achieving 1 km radar range with low-cost monolithic microwave integrated circuit (MMIC) based radar.

A. Related Work

A growing literature explores camera-based solutions for DAA [6]–[10]. However, much of the literature does not consider the problem of range estimation; it focuses instead on improving the detection and false alarm probabilities of the vision algorithms. The solutions for camera-based range estimation that do exist either perform poorly or impose unrealistic constraints:

1) *Contrast-to-Noise Ratio*: In [11], Minwalla and Ellis propose a DAA solution that leverages an array of narrow-field-of-view cameras. It uses a time series of contrast-to-noise ratios to estimate range, but the errors appear to be at least ± 1 km, which is unacceptably large [11]. Additionally, this method can be expected to be sensitive to atmospheric conditions such as fog and precipitation.

2) *Stereo Camera Triangulation*: Accurate depth sensing is difficult to achieve at long range because camera separation is limited to the size of the vehicle. This limitation introduces severe geometric dilution of precision at long range. This difficulty is compounded by airframe flexibility [12]. Consider, for example, stereo cameras separated by 10 m with a focal length of 4 mm and 4K resolution (3840×2160). Assume a target at 500 m. For these conditions, the range error per degree of camera misalignment is $440 \text{ m}/^\circ$, not accounting for noise in the cameras’ bearing estimates. These properties prompt Mcfayden and Mejias to dismiss stereo cameras as infeasible for DAA [12].

3) *Bearings-Only 3D Location Estimation*: Range can be observed under bearings-only tracking if the ego-aircraft “out-maneuvers” the target. But the large maneuvers required of the ego-aircraft, and the long filter convergence time (5–30s), render bearings-only unacceptable as a primary tracking method [12].

4) *Apparent Size*: Estimating range based on an object’s apparent size in an image requires knowledge of the physical size of the target object, which is generally not available [11], [12].

B. Deficiency in Existing Radar Solutions

Although radar is an obvious means of directly measuring range, current research in DAA for UAM avoids commercial radar units due to their poor SWaP-C characteristics [12]. For example, the EchoFlight Airborne Radar from Echodyne costs \$20k per unit, consumes 40 W, and has a mass of 800 g [13]. Moreover, three or four separate units would be required to obtain an adequate field of view. Thus, even if volume pricing reduced the unit price significantly, such products would impose a prohibitive strain on a VTOL's SWaP-C budget. A radar solution with low SWaP-C is highly desirable for designing a feasible DAA system for UAM.

Radar MMICs have recently become available under \$100 in 1000-unit volume pricing. For example, Analog Devices offers a chipset for the 24 GHz band which costs about \$70 in volume [14]. Such chips are targeted to automotive and industrial applications, but they could be adapted for UAM and UAL.

C. Adapting Low SWaP-C Radar for UAM and UAL

Due to their low power, radar systems built around these MMICs typically have ranges only up to 200 meters when operating in a traditional scanning mode. Their range must be increased to make them viable for use in UAM and UAL. It is possible to increase their range sensitivity beyond 1 km with greater transmit power and application of weak-signal correlation techniques in which the frequency-modulated continuous wave (FMCW) radar takes measurements over an extended interval (e.g., up to two seconds) at a chosen azimuth and elevation. Such measurement intervals make blind 2D scanning too slow, but can be effectively used to determine range to a target whose azimuth and elevation is already known.

This paper proposes a two-step technique for low SWaP-C DAA. First, a machine vision algorithm operates on visible light images to detect a target of interest and determine its azimuth and elevation relative to the ego-aircraft. Second, radar returns arriving from the detected direction are constructively combined to obtain a range estimate. The ego-aircraft then has enough information to infer the relative position of obstacles in the airspace. In the following sections, this technique is described in detail and analyzed for robustness to target velocity uncertainty. Experimental results with a low-cost radar chipset show that a typically-sized VTOL aircraft at 1 km range would be detectable.

D. Contributions

This paper makes two primary contributions. First, it develops a signal processing technique for extending the range of MMIC-based radar to 1 km, and analyzes the technique for sensitivity to target velocity uncertainty. Second, it reports experimental results that demonstrate the feasibility and effectiveness of the proposed technique. In so doing, this paper lays the foundation for implementing low SWaP-C, long-range radar for fused camera-radar systems. This is an important

step toward feasible and reliable DAA for UAM, UAL, and autonomous aviation in general.

II. THEORY

FMCW radar determines range to an object by emitting and receiving “chirp” signals, which are sinusoidal waveforms whose frequency increases linearly with time. While transmitting a chirp, the radar simultaneously receives the echo from that chirp. Because the chirp frequency increases linearly with time, the difference in frequency of the transmitted and received signals is proportional to the time-of-flight of the electromagnetic wave. This difference is therefore proportional to the distance to the reflecting object. This is illustrated in Fig. 1.

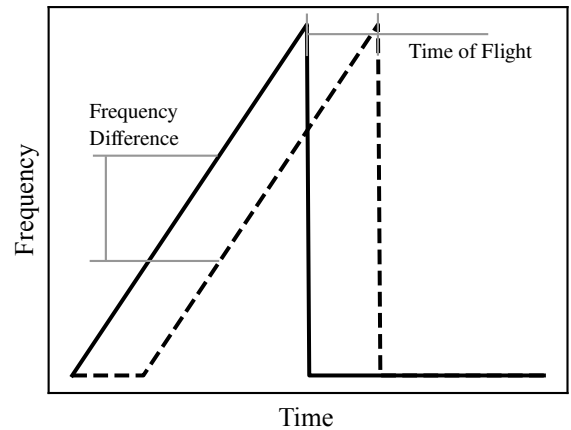


Fig. 1: FMCW chirp (solid) with corresponding echo (dashed). Longer time-of-flight corresponds to a greater frequency difference between the transmitted and received signals.

To measure this difference in frequency, the transmitted and received signals are mixed to obtain the so-called intermediate frequency (IF) signal. The IF contains beat frequencies for each reflecting target, which are detected in the frequency domain [15]. The frequency-domain IF signal will be referred to as the “range spectrum” because the frequency-domain bins correspond to discrete target ranges.

A. Optimizing FMCW Parameters for Range

The goal of this paper is to maximize the detection range of the radar by maximizing the signal-to-noise ratio (SNR) in the range spectrum. There are several ways to accomplish this SNR increase without increasing transmit power:

1) *Chirp Interval*: For a fixed sampling rate, SNR increases linearly with the chirp interval [15]. The size of hardware buffers can limit the maximum chirp interval. For example, the Inras RadarLog development kit [16] has a maximum buffer size of 10,240 samples. If the sampling rate is set at 2.5 Msps, this buffer size limits the chirp interval to a maximum of 4.096 ms.

2) *Filtering*: In addition to the signal of interest, the IF contains wideband noise. If there are known constraints on the frequency content of the signal of interest, then SNR can be increased by filtering out some of the noise. For example, if the IF is sampled by an ADC, then the signal of interest must reside below the Nyquist frequency of the ADC sampling rate. In this case, a lowpass filter can remove all of the noise power above the Nyquist frequency.

3) *Coherent Integration of Multiple Chirps*: The range spectra from multiple chirps can be summed coherently (retaining phase information in a complex sum) to increase SNR if the target signal's phase is consistent or predictable across the chirps. This causes the signal to add constructively, while the noise averages out to its mean. The result is that SNR increases by a factor of N , where N is the number of coherently-integrated chirps [17].

4) *Noncoherent Integration of Multiple Chirps*: When coherent integration is not possible (due to phase uncertainty), noncoherent integration may be performed by summing the magnitudes of range spectra from multiple chirps. This discards the phase information, and is therefore less efficient than coherent integration. Noncoherent integration increases SNR by a factor of K^α where K is the number of noncoherently-integrated chirps, and $\alpha \in (.5, 1)$ [17].

B. Limitations on Increasing SNR

The DAA application introduces two phenomena which limit the effectiveness of the SNR-increasing methods described above. Both of them are related to relative motion between the ego-aircraft and the target. Relative target motion is characterized by changes in range and bearing. Changes in bearing may be easily detected by the camera system and compensated for via simple beam steering. However, changes in range are more problematic.

1) *Doppler Effect*: If the target range changes over a chirp interval (non-zero radial speed), then the radar observes a Doppler shift. This introduces a ranging error because the radar infers range from the frequency of the received echoes. The ranging error e_d (meters) is approximated by

$$e_d = \frac{T_c}{\beta} f_0 v_r \quad (1)$$

where

T_c is the chirp time (s)

f_0 is the chirp center frequency (Hz)

v_r is the radial speed (m/s)

(positive for increasing range)

β is the chirp bandwidth (Hz)

Note that this expression is valid for “up-chirps” where the frequency vs. time slope is positive. The ranging error would be negated for down-chirps. This implies that a radar system could measure radial velocity by associating reflections from an up-chirp and a down-chirp [15]. Cancelling the Doppler effect in this way will be necessary in a practical system unless the target velocity is estimated by other means.

2) *Phase Drift*: The phase of a target's peak in the range spectrum depends on the distance between the transmit antenna and the target. Due to the short wavelength of the system (millimeters), the phase of this peak is sensitive to changes in target range [15]. If this target movement renders the phase inconsistent between chirps, then direct coherent integration is ineffective. The maximum measurement interval t_{\max} over which coherent integration between chirps is possible without phase correction is

$$t_{\max} = \frac{\theta_t c}{2\pi f_0 v_r} \quad (2)$$

where

$\theta_t \in (0, \frac{\pi}{2}]$ is the tolerated phase offset (rad)

c is the speed of light (m/s)

As an example, for $\theta_t = 1$ rad, $f_0 = 76$ GHz and $v_r = 50$ m/s, the coherent integration interval is about 13 μ s. Since the chirp intervals will be on the order of milliseconds in the DAA application, it is impossible to employ coherent integration by simply taking a complex sum over range spectra from different chirps. However, it is possible to perform coherent integration with a moving target if the phase drift can be corrected prior to integration. One such phase correction solution is presented in the following section.

III. PHASE CORRECTION

Coherent integration of multiple chirps is an efficient way to increase SNR, but direct coherent integration is not possible for the DAA application unless $v_r \approx 0$ m/s. Because v_r is almost always non-zero in practice, a method of phase correction is necessary to exploit the efficiency of coherent integration.

A “measurement interval” refers to the time over which chirps are collected for a single range estimate. For the purpose of phase correction, v_r is assumed to be constant over the measurement interval. Consider a sequence of N chirps. The range spectrum for each chirp contains a complex FFT coefficient in each of its range bins. The phases of these complex numbers are phase samples of the reflected signal. Because v_r is constant, the reflected signal's phase changes linearly with time. Assuming there is no dead time between the end of a chirp and the start of the next chirp, the phase drift from chirp to chirp is given (in rad/chirp) by

$$\omega = 2\pi \frac{v_r}{\lambda_0} T_c \quad (3)$$

where

λ_0 is the wavelength of the FMCW waveform (m)

T_c is the chirp time (s)

Without loss of generality, assign a phase of 0 rad to the first chirp in the sequence. Thus, each chirp in the sequence has a relative phase offset of

$$\phi(n) = \omega n \quad (4)$$

where $n \in \{0, 1, \dots, N-1\}$ is the chirp index.

Due to the modulo 2π property of phase offsets, all possible values of v_r can be described by $\omega \in [-\pi, \pi)$. In other words, the phase drift due to v_r is sampled every T_c seconds, which causes the phase-drift frequency ω to be aliased into the range $[-\pi, \pi)$ rad/chirp.

With this useful bound on ω , one can generate L hypotheses for the value of ω . To test each hypothesis, phase corrections (based on the hypothetical values of ω) are applied to the range spectra of N chirps. The goal is to find a hypothesis that “lines up” the phase of the signal in each range spectrum. The phase corrections for each hypothesis are given by

$$\bar{\phi}(n, l) = \frac{2\pi}{L}ln \quad (5)$$

where $l \in \{0, 1, \dots, L-1\}$ is the hypothesis index.

Thus, the hypotheses are spaced evenly in the interval $[-\pi, \pi)$ radians/chirp. Applying each hypothesis to the data yields corrected phase offsets of

$$\tilde{\phi}(n, l) = \phi(n) - \bar{\phi}(n, l) = \left(\omega - \frac{2\pi}{L}l\right)n \quad (6)$$

Note that

$$\min_l \left| \omega - \frac{2\pi}{L}l \right| \leq \frac{\pi}{L}$$

Therefore, under the best hypothesis, the phase offset between consecutive chirps is bounded by π/L . This further implies that the maximum phase offset between any two chirps in the group of N chirps is

$$\frac{\pi}{L}(N-1) \leq \theta_t \quad (7)$$

where $\theta_t \in (0, \frac{\pi}{2}]$ is the tolerated phase offset (rad) chosen by the designer.

Solving for L yields

$$L \geq \frac{\pi(N-1)}{\theta_t} \quad (8)$$

Therefore, given N chirps to coherently integrate and a requirement that their relative phases be within θ_t , the algorithm can generate L hypotheses with the guarantee that one of them will succeed in aligning the signal phases for coherent integration. Although this phase correction technique assumes that v_r is constant, it is still effective when v_r deviates slightly. This is demonstrated in Section IV-A.

In practice, M chirps are collected over a measurement interval, which may be up to two seconds long. Then, each hypothesis is applied to correct the phase of the chirp data. For each hypothesis, coherent integration is performed over contiguous groups of N chirps. This results in M/N “coherent groups,” which are then summed noncoherently. The detection algorithm is applied to each resulting composite range spectrum, and the hypothesis yielding the highest SNR is accepted as the best one.

The parameters M and N are chosen subject to system constraints such as available computational power, expected

target motion, and required SNR. M should be high enough to yield adequate SNR, but low enough that the constant v_r assumption remains valid. Similarly, increasing N increases SNR, but it also increases computational complexity. A larger N also necessitates larger L , which increases the probability of false alarm because it increases the likelihood that the phase of the noise matches one of the hypotheses. Thus, the optimal choice of M and N strongly depends on the system characteristics.

A. Angle of Arrival Selection

The FMCW processor operates on signals from a specific azimuth and elevation determined by cameras. This relaxes the computational demands of the signal processing, allowing more time for the SNR-increasing techniques mentioned above. Consider a one-dimensional phased-array radar system that takes n_s samples of each chirp to detect k targets. In a typical phased array, azimuth is deduced from the phase offset between multiple receive antennas. Algorithmically, this is achieved with a fast Fourier transform (FFT) taken over the receive antennas. The resulting FFT bins correspond to different bearings. If the targets are assumed sparse, then the FFT may be zero-padded to achieve super-resolution. Let m be the length of the azimuth-resolving FFT. Note that m is lower-bounded by the number of receive antennas. Further, suppose l_a one-dimensional arrays are “stacked” to cover a discrete range of elevations.

Standard Method: If the IF for each receiving antenna has already been transformed to the frequency domain, an operation that requires $O(n_s \log(n_s))$ time, then generating azimuth data from a single chirp for the entire radar scene is possible with computational complexity $T'(m, l_a, n_s) \in O(m \log(m)n_s l_a)$. Thus, the total computational complexity of “blind 2D scanning” is

$$T(m, l_a, n_s) \in O(n_s \log(n_s) + m \log(m)n_s l_a) \quad (9)$$

Proposed Method: If, however, the azimuths and elevations of the k targets are available from cameras, then a particular azimuth and elevation can be selected in the signal processing. The azimuth can be selected by simply multiplying each antenna’s IF by an expected phase offset and summing them. Elevation is selected by only accepting input from the appropriate array. Determining the range of all the targets with this method implies computational complexity $T'(k, n_s) \in O(kn_s)$, so the total complexity for a single chirp in this case is

$$T(k, n_s) \in O(n_s \log(n_s) + kn_s) \quad (10)$$

In addition, the angle-selection method allows the detection algorithm to operate on k one-dimensional range spectra rather than a three-dimensional range spectrum, which yields further computational savings.

IV. EXPERIMENTAL RESULTS

The range-extending approach was implemented and tested with the Inras RadarLog, a development platform for 77 GHz radar [16]. Note that the techniques explored in this paper

are transferrable to the 24 GHz band, which is preferred for aviation in the United States due to FCC regulations [18]. To simulate in-flight conditions, the RadarLog was placed face-up on the ground in an open field. An unmodified DJI Mavic 2 Pro drone [19] was flown directly above the RadarLog at various altitudes to act as the target. See Fig. 2 for a photo of the experimental hardware. The radar was tested at several altitudes up to 120 m. At each altitude, the drone was commanded to hover. Wind conditions were mild, resulting in favorable conditions for reducing target velocity uncertainty. The drone would have been detectable beyond 120 m, but FAA regulations do not allow remote pilots to operate above that altitude without a waiver.

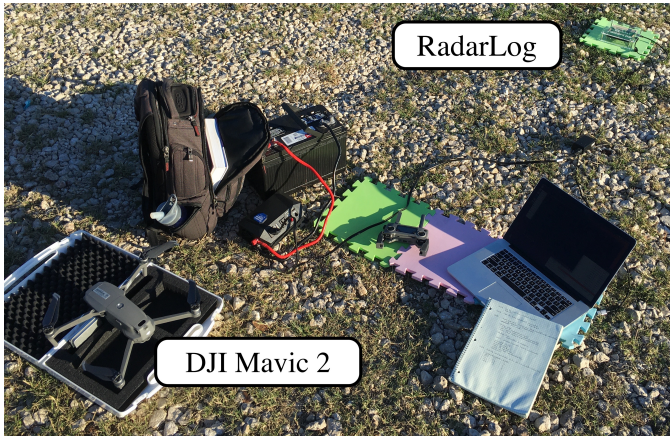


Fig. 2: Experimental hardware: the RadarLog unit rests on a ground pad in the upper right corner of the photo. An unmodified DJI Mavic 2 was flown up to an altitude of 120 m to act as a target.

TABLE I: Chirp configurations tested at each altitude. Note that the number of chirps for each configuration was adjusted to maintain a constant measurement interval. In other words, the same amount of data was collected for each chirp configuration. The chirps were summed noncoherently to produce the results in Fig. 3.

Chirp Interval (μs)	Buffer Length	Number of Chirps	Total Measurement Interval (s)
4096	10240	256	1.049
2048	5120	512	1.049
1024	2560	1024	1.049
512	1280	2048	1.049
256	640	4096	1.049

Chirp parameters were chosen based on the theoretical development in Section II. These considerations resulted in a low sampling rate of 2.5 Msps and a maximum chirp length of 10240 samples over 4.096 ms. See Table I for a list of all tested configurations. These configurations were tested on the target UAV at 20 m increments up to an altitude of 120 m. The results of this experiment are shown in Fig. 3. Only data points for which the drone was detectable are plotted.

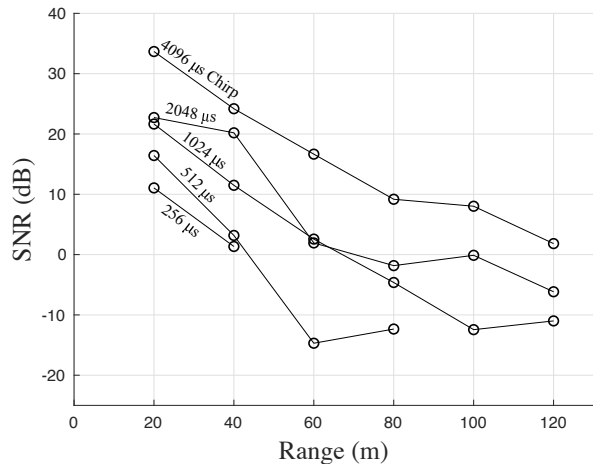


Fig. 3: SNR of the radar return at various ranges and chirp configurations. Noise power was estimated from control data which was recorded with no target present. This noise estimate was used to calculate SNR.

Notice that, for the most part, the shorter chirp intervals yield lower SNR despite the constant measurement intervals. This happens because an FMCW chirp is intrinsically coherent, and therefore more efficient at raising SNR than the noncoherent integration used to combine separate chirps. In general, a few long chirps will yield higher SNR than many short chirps over equivalent measurement intervals. In practice, chirp length is limited by non-constant v_r , which causes the reflected signal energy to spread over multiple range bins.

A. Phase Correction Results

The phase correction method described in Section III was applied to the experimental data. The results for a chirp length of 1024 μs and a target range of 120 m are shown in Figs. 4 and 5. Fig. 4 shows the raw (uncorrected) phase values taken from the range spectra of each chirp. Phase corrections from the best hypothesis are overlaid on the graph. The nonlinearity of the phase is apparent in Fig. 4, but the phase correction technique still yields significant SNR gain, as depicted in Fig. 5. The increase in SNR of 20 dB is substantial, and it demonstrates the effectiveness of the phase correction technique.

V. EXTRAPOLATION OF RESULTS

The foregoing experimental results can be extrapolated to infer the performance of a real system designed with the same techniques. Consider how target radar cross section (RCS) and transmit power would change upon application of this paper’s techniques to UAM:

1) *Radar Cross Section*: Radar cross section is a measure of a radar target’s reflectivity. The signal power in watts that a radar receives from a target is given by [15]

$$P_{RX} = \frac{P_{TX} G_{TX} \sigma A_{RX}}{(4\pi)^2 d^4} \quad (11)$$

where

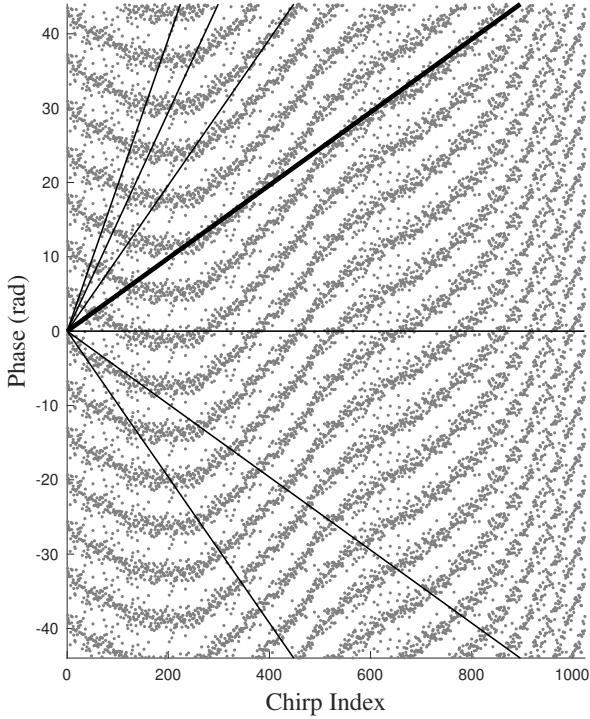


Fig. 4: Gray points indicate the raw phase of each range bin corresponding to the target range (120 m). Each phase measurement is vertically replicated every 2π radians to reveal contours in the plot. The thick black line represents the best phase-correction hypothesis, and the thin lines are adjacent hypotheses. Note that the chosen hypothesis most closely matches the phase contours. For this plot, $M = 1024$, $N = 64$, $L = 128$, and $\theta_t = \pi/2$.

P_{TX} is the transmit power (W)
 G_{TX} is the transmit antenna gain (dimensionless)
 σ is the RCS of the target (m^2)
 A_{RX} is the effective aperture of the receive antenna (m^2)
 d is the distance to the target (m)

An object's RCS is often difficult to calculate because it depends on many factors, including shape, material, size, and orientation. For the purpose of this analysis, assume that RCS scales linearly with geometric cross section. The DJI drone in this experiment has overall horizontal dimensions of $0.322 \text{ m} \times 0.242 \text{ m}$ [19].

Joby Aviation, a leader in VTOL technology, recently unveiled their VTOL airframe, which has a wingspan of 10.7 m [20]. Assume the height is 3 m . Under these assumptions, the ratio of geometric cross sections (front of Joby's airframe to the bottom of the DJI drone) is about

$$\frac{\Sigma_{\text{Joby}}}{\Sigma_{\text{DJI}}} \approx \frac{10.7 \text{ m} \times 3 \text{ m}}{0.322 \text{ m} \times 0.242 \text{ m}} \approx 412$$

According to (11), this increase in RCS translates to a factor

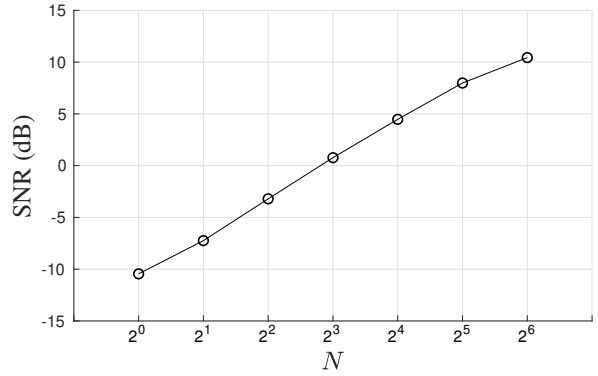


Fig. 5: SNR of radar return after phase-corrected coherent integration. Recall that N denotes the number of chirps coherently integrated in each group. The groups are added noncoherently. For this plot, $\theta_t = \pi/2$. The values of N were chosen simply to demonstrate the effectiveness of the phase correction technique. Larger values may be used depending on the system characteristics and capabilities.

of

$$\sqrt[4]{\frac{\Sigma_{\text{Joby}}}{\Sigma_{\text{DJI}}}} \approx 4.5$$

range increase.

The RadarLog detected the DJI drone at 120 m using only noncoherent integration, so it can be expected to detect a typically-sized VTOL aircraft at 540 m under similar conditions with no modification to the hardware. By (11), doubling this 540 m range would require an SNR increase of 12 dB . The results in section IV-A indicate that a 12 dB increase in SNR is possible with phase correction. Thus, 1 km range is achievable with the hardware used in this experiment.

2) *Transmit Power*: The RadarLog currently transmits at 10 dBm . A fully-implemented system could increase transmit power if allowed by the SWaP-C budget. This would increase overall performance and allow detection of targets in more challenging conditions.

VI. CONCLUSIONS

As the aerospace industry races to produce a viable autonomous aircraft for urban environments, the need increases for an inexpensive and reliable detect and avoid (DAA) system. Autonomous systems need to match a human pilot's DAA performance, but this has not been accomplished yet [4]. Visible light cameras are useful for DAA, but cameras alone are insufficient because of their fundamental inability to accurately resolve range. Low SWaP-C radar is a necessary component of DAA systems because it provides range measurements to complement angular measurements provided by cameras.

A low SWaP-C radar solution has been developed and tested for autonomous DAA systems. The method employs weak-signal correlation techniques and long measurement intervals to extend the range of existing low SWaP-C radar chipsets.

Because blind 2D scanning would be too slow with the required signal processing, the radar only processes signals from particular directions identified by cameras. The radar portion of this system was tested with an Inras RadarLog development kit, and the results show that a typically-sized VTOL aircraft at 1 km range would be detectable if a full-scale system were implemented. This type of low SWaP-C radar will facilitate the development of a feasible DAA system and accelerate the widespread adoption of autonomous urban air mobility.

[20] Vertical Flight Society, “Joby S4.” <https://evtol.news/aircraft/joby-aviation/>, Jan. 2020.

REFERENCES

- [1] D. P. Thippavong, R. Apaza, B. Barmore, V. Battiste, B. Burian, Q. Dao, M. Feary, S. Go, K. H. Goodrich, J. Homola, *et al.*, “Urban air mobility airspace integration concepts and considerations,” in *2018 Aviation Technology, Integration, and Operations Conference*, p. 3676, 2018.
- [2] J. Holden and N. Goel, “Uber elevate: Fast-forwarding to a future of on-demand urban air transportation,” *Uber Inc., San Francisco, CA*, 2016.
- [3] W. C. Barott, E. Coyle, T. Dabrowski, C. Hockley, and R. S. Stansbury, “Passive multispectral sensor architecture for radar-EOIR sensor fusion for low SWaP UAS sense and avoid,” in *2014 IEEE/ION Position, Location and Navigation Symposium-PLANS 2014*, pp. 1188–1196, IEEE, 2014.
- [4] J. James, J. J. Ford, and T. L. Molloy, “Learning to detect aircraft for long-range vision-based sense-and-avoid systems,” *IEEE Robotics and Automation Letters*, vol. 3, no. 4, pp. 4383–4390, 2018.
- [5] S. Smearcheck, S. Calhoun, W. Adams, J. Kresge, and F. Kunzi, “Analysis of alerting performance for detect and avoid of unmanned aircraft systems,” in *2016 IEEE/ION Position, Location and Navigation Symposium (PLANS)*, pp. 710–730, IEEE, 2016.
- [6] J. James, J. J. Ford, and T. L. Molloy, “Below horizon aircraft detection using deep learning for vision-based sense and avoid,” *arXiv preprint arXiv:1903.03275*, 2019.
- [7] C. M. Geyer, D. Dey, and S. Singh, “Prototype sense-and-avoid system for UAVs,” Tech. Rep. CMU-RI-TR-09-09, Carnegie Mellon University, Pittsburgh, PA, May 2009.
- [8] J. James, J. J. Ford, and T. L. Molloy, “Quickest detection of intermittent signals with application to vision-based aircraft detection,” *IEEE Transactions on Control Systems Technology*, vol. 27, no. 6, pp. 2703–2710, 2018.
- [9] J. Lai, J. J. Ford, L. Mejias, and P. O’Shea, “Characterization of sky-region morphological-temporal airborne collision detection,” *Journal of Field Robotics*, vol. 30, no. 2, pp. 171–193, 2013.
- [10] D. Bratanov, L. Mejias, and J. J. Ford, “A vision-based sense-and-avoid system tested on a scaneagle uav,” in *2017 International Conference on Unmanned Aircraft Systems (ICUAS)*, pp. 1134–1142, IEEE, 2017.
- [11] C. Minwalla and K. Ellis, “Experimental evaluation of PICAS: An electro-optical array for non-cooperative collision sensing on unmanned aircraft systems,” in *AIAA Information Systems-AIAA Infotech@ Aerospace*, p. 0907, 2017.
- [12] A. Mcfadyen and L. Mejias, “A survey of autonomous vision-based see and avoid for unmanned aircraft systems,” *Progress in Aerospace Sciences*, vol. 80, pp. 1–17, 2016.
- [13] Echodyne, “EchoFlight airborne radar.” <https://echodyne.com/products/echoflight/>, Sept. 2019.
- [14] J. Morrissey and P. Walsh, “High performance integrated 24 GHz FMCW radar transceiver chipset for auto and industrial sensor applications.” <https://www.analog.com/en/technical-articles/integrated-24-ghz-fmcw-radar-transceiver-chipset.html>, Jan. 2020.
- [15] S. Rao, “Introduction to millimeter-wave sensing: FMCW radars,” *Texas Instruments (TI) Millimeter-Wave Training Series*, 2017.
- [16] INRAS, “Products.” <http://www.inras.at/en/products.html>, Jan. 2020.
- [17] M. A. Richards, “Noncoherent integration gain, and its approximation,” *Georgia Institute of Technology, Technical Memo*, 2010.
- [18] Federal Communications Commission, “47 CFR Part 15.253: Operation within the bands 46.7–46.9 GHz and 76.0–77.0 GHz.” Federal Register, Oct. 2000.
- [19] DJI, “MAVIC 2 specifications.” <https://www.dji.com/mavic-2/info>, Jan. 2020.